*Geophys. J. Int.* (2008) **173,** 802–805 doi: 10.1111/j.1365-246X.2008.03795.x

FAST TRACK PAPER

# A gravity gradient method for characterizing the post-seismic deformation field for a finite fault

T. J. Hayes,[1] K. F. Tiampo,[1] J. Fernández[2] and J. B. Rundle[3]

[1] *Department of Earth Sciences, The University of Western Ontario, London, Ontario, Canada. E-mail: thayes@uwo.ca*
[2] *Institutio de Astronomía y Geodesia (CSIC-UCM), Fac. CC. Matemáticas, Ciudad Universitaria, Spain*
[3] *Center for Computational Science and Engineering, University of California, Davis, California, USA*

Accepted 2008 March 17. Received 2008 March 17; in original form 2007 October 28

## SUMMARY

Gravity gradients are an effective method for delineating the extent of subsurface density anomalies. The change in subsurface density contrasts due to the seismic deformation gives rise to detectable gravity changes via the dilatational gravity signal or Bouguer anomaly. Solutions for the corresponding gravity gradients of these signals are developed for a vertical strike-slip fault. Gravity gradient solutions exhibit similar spatial distributions as those calculated for Coulomb stress changes, reflecting their physical relationship to the stress changes. The signals' magnitudes, of the order of $10^{-4}$ E, are beyond the resolution of typical exploration instruments. Improvements to Superconducting Gravity Gradiometers are necessary for gravity gradients to be used as a viable method for the observation of the stress field changes over large spatial scales.

**Key words:** Numerical solutions; Seismic cycle; Time variable gravity; Earthquake interaction, forecasting, and prediction.



## 1 INTRODUCTION

The analytic solutions of the deformation field from seismic events are well established in the literature for elastic half-spaces (Chinnery 1963; Mansinha & Smylie 1971; Okada 1985) and further developed for the corresponding stress and strain fields (Okada 1992). Seismic triggering studies that interpret the Coulomb stress changes arising from the resultant deformation field after a seismic event, have demonstrated the potential for identifying regions of future seismic activity (King *et al.* 1994; Stein *et al.* 1994; Freed & Lin 2001). However, the Coulomb stress changes are inherently unobservable by direct measurement and are typically restricted to surface observations; their values at focal depths must be inferred.

By contrast with stress and strain measurements, gravity observations record changes from all depths and their acquisition over large spatial scales is common due, in large part, to their extensive use in exploration geophysics. The analytic solutions for the gravity changes from an earthquake were first numerically solved for by Rundle (1978), and analytically solved for a thrust fault and dilatational point source by Walsh & Rice (1979). Okubo (1991, 1992) developed the general solutions for a finite fault within a half-space, which was further extended for complex fault networks by Hayes *et al.* (2006). Walsh & Rice (1979) explicitly derive the dilatational solutions in terms of the stresses induced in the subsurface medium, and as demonstrated by Okubo (1992), the dilatational, or Bouguer, gravity anomaly corresponds directly to the subsurface density from seismic activity. Often, of more practical use in exploration geophysics are the gravity gradients, which delineate the edges of subsurface density anomalies (Bell 1997; Saad 2006). As such, it follows that the gravity gradients may provide more detailed information on the spatial distribution of the deformation field following an earthquake and, in turn, its subsurface stress and strain.

The purpose of this paper is to provide the analytic gravity gradient solutions for a vertical strike-slip finite fault within an elastic half-space. In Section 2, we outline our method and solutions. Section 3 shows the results for several of the gradient solutions followed by a discussion of the results in Section 4.

## 2 THE GRAVITY GRADIENT SOLUTIONS

To calculate the gravity gradient changes for an earthquake, we first use the potential Green's functions developed by Okubo (1992). In general, the expressions used for the dilatational gravity potential changes are given by

$$\Delta P*(x_1, x_2, x_3) = \{\rho G[U_1 S^*(\xi, \eta) + U_2 D^*(\xi, \eta) + U_3 T^*(\xi, \eta)] + \Delta\rho G U_3 C^*(\xi, \eta)\}\|, \quad (1)$$

where $\rho$ is the density of the medium, $G$ is Newton's Universal gravitational constant, $\xi$ and $\eta$ are coordinates on the fault length and width, respectively and $U_i$ is the slip vector. We have used the double vertical notation of Chinnery (1961). For our analysis, we need only focus on the strike-slip component, where $S^*$ $(\xi, \eta)$ is

given by,

$$S^*(\xi,\eta) = (1-2\nu)\tan\delta\{-R - 2\xi I_1 \tan\delta + q\sec\delta[\sin\delta\cdot\log(R+\eta) - \log(R+\bar{d})]\}, \quad (2)$$

and note that,

$$I_1(\xi,\eta) = \tan^{-1}\left[\frac{-q\cos\delta + (1+\sin\delta)(R+\eta)}{\xi\cos\delta}\right]. \quad (3)$$

In expressions (1)–(3), $\nu$ is Poisson's ratio, $d$ is the depth to the bottom of the fault beneath the origin and $\xi \equiv x_1 - \xi'$ and $\eta \equiv p - \eta'$, where

$$p \equiv x_2\cos\delta + (d - x_3)\sin\delta,$$
$$R \equiv \sqrt{\xi^2+\eta^2+q^2},$$
$$q = x_2\sin\delta - (d-x_3)\cos\delta,$$
$$\bar{d} = \eta\sin\delta - q\cos\delta.$$

See Okubo (1992), fig. 2, for a complete description of the coordinate system used.

To calculate the gravity gradients, we first define the operators for the potential Green's function given by (1), which simplify to the following expressions for a vertical strike-slip fault,that is, $\cos\delta = 0$.

$$\frac{\mathrm{d}}{\mathrm{d}x_1} = \frac{\partial\xi}{\partial x_1}\frac{\partial}{\partial\xi}\,|_{x_3=0},$$
$$\frac{\mathrm{d}}{\mathrm{d}x_2} = \frac{\partial q}{\partial x_2}\frac{\partial}{\partial q}\,|_{x_3=0},$$
$$\frac{\mathrm{d}}{\mathrm{d}x_3} = -\frac{\partial p}{\partial x_3}\frac{\partial}{\partial\eta}\,|_{x_3=0}. \quad (4)$$

In general, the above operators can be used on the gravity potential solutions in eq. (1) (hereafter, simply denoted as $P$) to find the horizontal gravity solutions, as well as their respective gradients for vertical strike-slip systems. Of the nine solutions for the full gravity gradient tensor, five are independent. The independent solutions are: $P_{xx}$, $P_{xy} = P_{yx}$, $P_{zx} = P_{xz}$, $P_{zy} = P_{yz}$ and $P_{zz}$, where the subscripts indicate the derivatives and $x = x_1$, $y = x_2$, $z = x_3$ using the coordinate system of Okubo (1992). The final dependent solution, $P_{yy}$ can be found using Laplace's equation where, $P_{yy} = -P_{xx} - P_{zz}$ for a closed system (Walsh & Rice 1979).

For the purposes of this paper, we provide the $x_1$, $x_2$, and $x_3$ Green's function gravity gradients,that is, the vertical gravity gradient, $\mathrm{d}^2P/\mathrm{d}x_3^2 = P_{zz}$, and the horizontal gravity gradients, $\mathrm{d}^2P/\mathrm{d}x_3\,\mathrm{d}x_1 = P_{zx}$ and $\mathrm{d}^2P/\mathrm{d}x_3\mathrm{d}x_2 = P_{zy}$, using eq. (1) for a vertical strike-slip fault. For this case where $\cos\delta = 0$, we find the following expressions for the gravity gradient Green's functions.

$$S^*_{zz}(\xi,\eta) = (1-2\nu)\frac{q}{R(R+\eta)}, \quad (5)$$

$$S^*_{zx}(\xi,\eta) = (1-2\nu)\frac{q\xi}{R(R+\eta)^2}, \quad (6)$$

$$S^*_{zy}(\xi,\eta) = -(1-2\nu)\left[\frac{1}{R+\eta} - \frac{q^2}{R(R+\eta)^2}\right]. \quad (7)$$

## 3 RESULTS

Using the Green's functions (5)–(7) in (1), we can calculate the gravity gradient solutions for a vertical strike-slip fault. In Fig. 1, we plot the vertical gravity gradient using eq. (5) for a right-lateral strike-slip fault. The vertical gravity gradient exhibits a similar antisymmetric butterfly pattern as that for the dilatational gravity (See Okubo 1992, fig. 4).

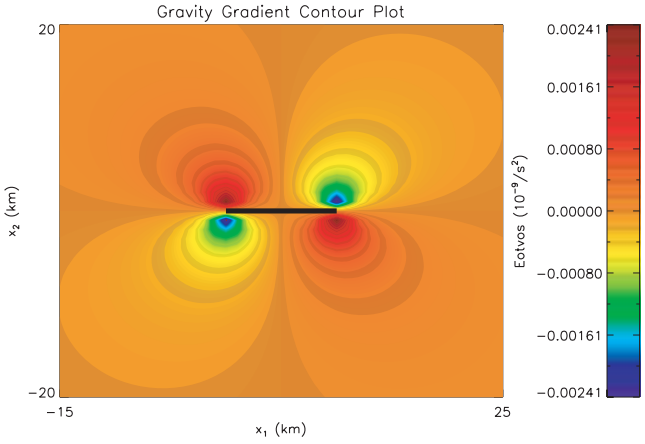


**Figure 1.** The vertical gravity gradient for a vertical right-lateral strike-slip fault. $L = 10$ km, $W = 10$ km, depth to the top of the fault is 1 km, and the dislocation is 5 m. The units are in Eötvös (E), which is equivalent to 0.1 μ Gal m$^{-1}$ or $10^{-9}$ s$^{-2}$. The thick black line is the location of the fault.

For the horizontal gradients, we make note of the fact that they are coordinate dependent, and thus their derivatives are dependent upon the direction in which their derivatives are found. The consequence of this is that derivatives in either the positive or the negative direction will produce similar spatial patterns but with opposite signs. As such, we plot only the magnitude of the horizontal components. We further note that we have employed the use of the more common unit for gravity gradients in exploration geophysics, that is, the Eötvös (E), where 1 E = 0.1 μGal m$^{-1}$ or $10^{-9}$ s$^{-2}$ in S.I. units.

In Figs 2(a) and (b), the solutions to (6) and (7) are shown, respectively. The $y$-component of the gravity gradient has a larger magnitude than the corresponding $x$-component of the gravity gradient; however, the pattern produced by the $x$-component exhibits a more diverse topology and spatially complex signal.

A common technique in exploration geophysics is to examine the various combinations of the gravity gradients to further delineate the extent of the subsurface density anomaly. We examine here a linear combination of eqs (5)–(7). In Fig. 3, we present two cases where we have added the components of the gravity gradient in the following manner,

$$\epsilon\, P^* - P_{zx}, \quad (8)$$

where $\epsilon$ is used as a dimensionless scaling factor, from 0 to 1, and $P^* = P_{zz} + P_{zy}$. The scaling factor is used to generate comparable magnitudes of the $z$- and $y$-components of the gravity gradient to the smaller $x$-component values, which would otherwise be masked by these stronger signals.

In Fig. 3, we demonstrate how the effect of the scaling factor, $\epsilon$, affects the resulting spatial distribution of the signal. As expected, smaller value of $\epsilon$ in Fig. 3(a) yields a signal with a greater component of the horizontal gravity gradient in the $x$-direction. This has the effect of retaining the slight negative values in the top-left-hand side and bottom-right-hand side quadrants of the signal. The larger $\epsilon$ value in Fig. 3(b) almost masks these signals completely.

Using the source parameters and fault dimensions for the Joshua Tree earthquake, as given by Bennett *et al.* (1995), we apply the gravity gradient solution in eq. (8) with $\epsilon = 0.035$. For comparison purposes, we also provide the Coulomb stress change in Fig. 5 using

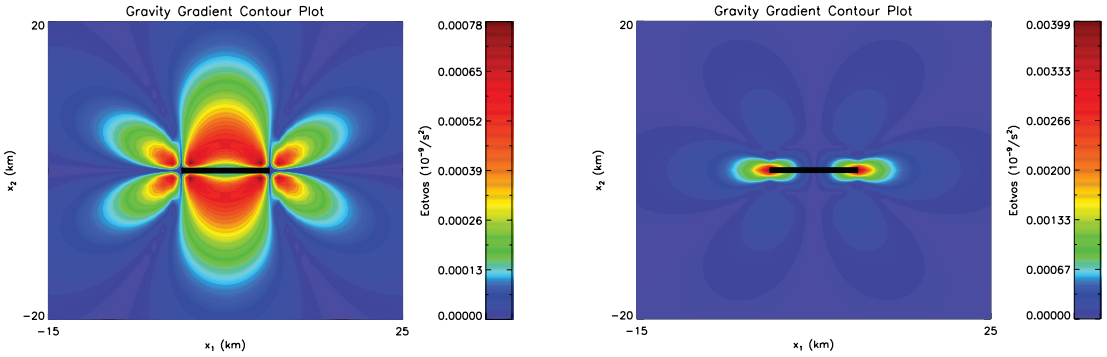


**Figure 2.** (a) The *x*-horizontal gravity gradient magnitude for a vertical right-lateral strike-slip fault and (b) the *y*-horizontal gravity gradient magnitude. Parameters used in (a) and (b) are the same as those used in Fig. 1. Note that the scales are different in (a) and (b).

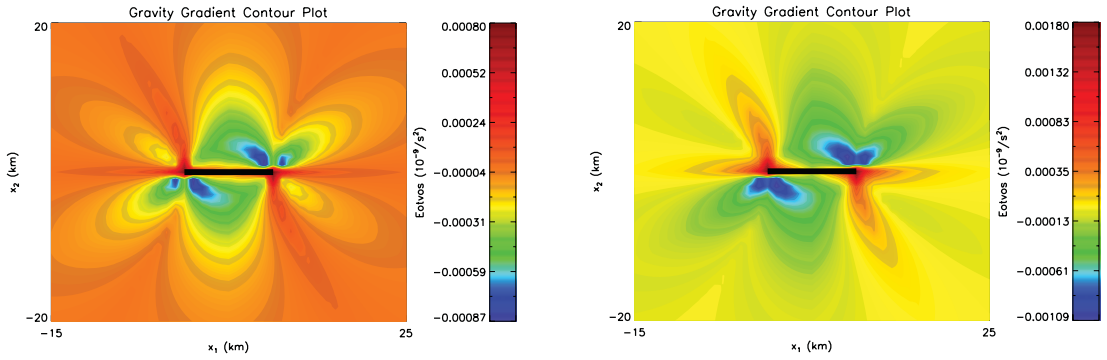


**Figure 3.** The gravity gradient solution given by eq. (8) with (a) $\epsilon = 0.15$ and (b) $\epsilon = 0.4$. Parameters are the same as those used in Fig. 1. Note that the scales are different in (a) and (b).

the Coulomb 3.0 software (Lin & Stein 2004; Toda *et al.* 2005). It should be noted that, to have a more consistent comparison with Fig. 4, Fig. 5 does not include the regional stress component, as it is currently not included in the gradient solutions.

We observe similarities in the spatial distribution for the gravity gradient plot of Fig. 4 and the Coulomb stress change plot of Fig. 5. Moreover, we note that by using eq. (4) we solve for the expected gravity gradient solution at the surface, whereas the Coulomb stress changes are calculated at depth.

## 4 DISCUSSION

Using the gravity gradients to delineate the edges of subsurface density anomalies, we have provided the gravity gradient Green's function solutions for the subsurface density anomalies in the post-seismic regime for a vertical strike-slip fault. The physical relationship between the gravity gradients and the corresponding Coulomb stress changes for the deformation field of a finite, strike-slip fault is clearly evident in the similar spatial distributions of Figs 3 and 4, respectively. Moreover, Walsh & Rice (1979) have shown explicitly that the gravity solutions for a dilatational point source and dip-slip fault can be found in terms of the stress changes following seismic events.

As such, the use of gravity gradients may offer researchers the ability to map the actual Coulomb stress changes by using the

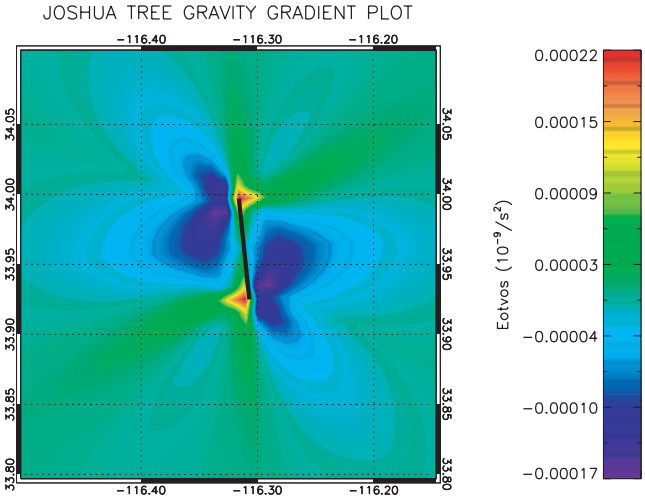


**Figure 4.** The gravity gradient solution of eq. (8) for the 1992 April Joshua Tree earthquake. The parameters are $L = 8$ km, $W = 10$ km, with a right-lateral dislocation of 0.8 m and an $\epsilon$ value of 0.35. To avoid singularities, the depth to the top of the fault is 500 m. The thick black line indicates the approximate location of the Joshua Tree Fault.

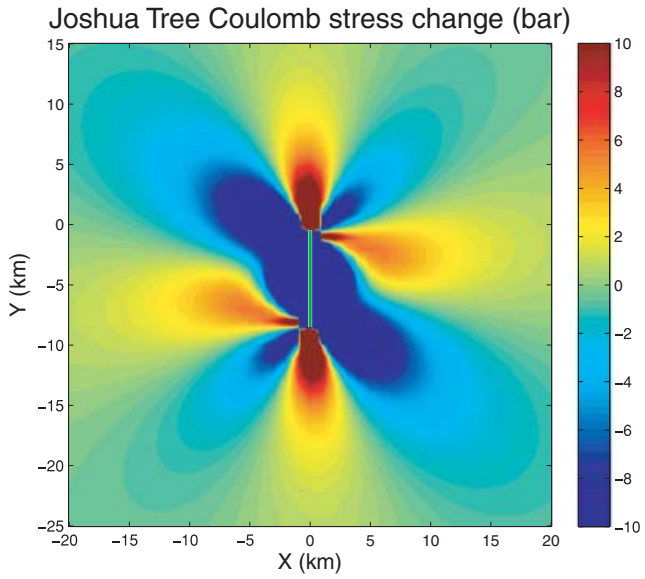


**Figure 5.** The Coulomb stress change for the 1992 April Joshua Tree earthquake. The parameters used are the same as in Fig. 4, calculated at a depth of 8 km and using a coefficient of friction value of 0.40. The thin green line indicates the approximate location of the Joshua Tree fault.

gradients as a proxy for the stress changes in the system. Furthermore, we suggest this may offer a practical complement to the traditional suite of seismic hazard assessment tools such as combined InSAR and GPS methods (Samsonov & Tiampo 2006) and statistical seismicity methods (Bowman & King 2001; Tiampo *et al.* 2002), in addition to traditional Coulomb stress change solutions (King *et al.* 1994; Freed & Lin 2001).

Exploration techniques of the 1930s commonly yielded gravity gradient resolutions of the order of magnitude of $\pm$ 1 E (Bell 1997), and recent developments in quantum-based instruments promise improved sensitivity in the near future. Moody *et al.* (2003) are developing an instrument for use in an aircraft or ship with an accuracy of $<1\,\mathrm{E\,Hz^{-1/2}}$. Superconducting Gravity Gradiometer (SGG) designs for space-borne missions, which require $10^{-4}\,\mathrm{E\,Hz^{-1/2}}$ sensitivity, have been demonstrated to achieve $0.02\,\mathrm{E\,Hz^{-1/2}}$ in the lab. Enhancements to the SGG, for example, by employing magnetically suspended test masses (versus the current mechanical suspension), may provide improved sensitivity by several orders of magnitude yielding resolutions of $10^{-5}\,\mathrm{E\,Hz^{-1/2}}$ (Moody *et al.* 2002).

We suggest that highly sensitive SGGs, designed for constant terrestrial observation, may allow for the measurement of the post-seismic gravity gradient changes arising from large events such as the Joshua Tree–Landers–Hector Mine sequence. Plans to incorporate the underlying regional stress, as well as more complex fault geometries, are underway. Moreover, extension of the method to include thrusting fault solutions, which contain larger gravity signals than strike-slip faults, may produce more readily observed signals.

## ACKNOWLEDGMENTS

The research of TJH was funded by the Ontario Graduate Scholarship, the Lucien LaCoste Scholarship from the Society of Exploration Geophysicists and Earth Researcher Award ER05-01-121. The research of KFT was funded by the NSERC and Benfield/ICLR IRC in Earthquake Hazard Assessment and by an NSERC Discovery Grant. Research by JF has been supported by Spanish MEC project CGL2005-05500-C02. The work of JBR has been supported by a grant from US Department of Energy, Office of Basic Energy Sciences to the University of California, Davis DE-FG03-95ER14499, with additional funding from the National Aeronautics and Space Administration under grants to the University of California, Davis.

## REFERENCES

Bell, R.E., 1997. Gravity gradiometry resurfaces, *Leading Edge,* **16,** 1, 55–59.

Bennett, R.A., Reilinger, R.E., Rodi, W., Li, Y., Toksöz, M.N. & Hudnut, K., 1995. Coseismic fault slip associated with the 1992 $m_w$ 6.1 Joshua Tree, California, earthquake: implications for the Joshua Tree–Landers earthquake sequence, *J. geophys. Res.,* **100**(B4), 6443–6461.

Bowman, D.D. & King, G.C.P., 2001. Accelerating seismicity and stress accumulation before large earthquakes, *Geophys. Res. Lett.,* **28,** 4039–4042.

Chinnery, M.A., 1961. The deformation of the ground around surface faults, *Bull. seism. Soc. Am.,* **51**(3), 355–372.

Chinnery, M.A., 1963. The stress changes that accompany strike-slip faulting, *Bull. seism. Soc. Am.,* **53**(5), 921–932.

Freed, A.M. & Lin, J., 2001. Delayed triggering of the 1999 Hector Mine earthquake by viscoelastic stress transfer, *Nature,* **411,** 180–183.

Hayes, T.J., Tiampo, K.F., Rundle, J.B. & Fernández, J., 2006. Gravity changes from a stress evolution earthquake simulation of California, *J. geophys. Res.,* **111,** B09408.

King, G.C.P., Stein, R.S. & Lin, J., 1994. Static stress changes and the triggering of earthquakes, *Bull. seism. Soc. Am.,* **84**(3), 935–953.

Lin, J. & Stein, R.S., 2004. Stress triggering in thrust and subduction earthquakes, and stress interaction between the southern San Andreas and nearby thrust and strike-slip faults, *J. geophys. Res.,* **109,** B02303.

Mansinha, L. & Smylie, D.E., 1971. The displacement fields of inclined faults, *Bull. seism. Soc. Am.,* **61**(5), 1433–1440.

Moody, M., Paik, H.J. & Canavan, E.R., 2002. Three-axis superconducting gravity gradiometer for sensitive gravity experiments, *Rev. Sci. Instrum.,* **73,** 3957–3974.

Moody, M., Paik, H.J. & Canavan, E.R., 2003. Three-axis superconducting gravity gradiometer for sensitive gravity experiments, *Rev. Sci. Instrum.,* **74,** 1310–1318.

Okada, Y., 1985. Surface deformation due to shear and tensile faults in a half-space, *Bull. seism. Soc. Am.,* **75**(4), 1135–1154.

Okada, Y., 1992. Internal deformation due to shear and tensile faults in a half-space, *Bull. seism. Soc. Am.,* **82**(2), 1018–1040.

Okubo, S., 1991. Potential and gravity changes raised by point dislocations, *Geophys J. Int.,* **105,** 573–586.

Okubo, S., 1992. Gravity and potential changes due to shear and tensile faults in a half space, *J. geophys. Res.,* **97**(B5), 7137–7144.

Rundle, J.B., 1978. Gravity changes and the Palmdale uplift, *Geophys. Res. Lett.,* **5**(1), 41–44.

Saad, A.H., 2006. Understanding gravity gradients—a tutorial, *Leading Edge,* **25,** 8, 942–949.

Samsonov, S. & Tiampo, K., 2006. Analytical optimization of a DInSAR and GPS dataset for derivation of three-dimensional surface motion, *IEEE Geosci. Remote Sens. Lett.,* **3**(1), 107–111.

Stein, R.S., King, G.C.P. & Lin, J., 1994. Stress triggering of the 1994 $m =$ 6.7 Northridge, California, earthquake by its predecessors, *Science,* **265,** 1432–1435.

Tiampo, K.F., Rundle, J.B., McGinnis, S.A. & Klein, W., 2002. Pattern dynamics and forecast methods in seismically active regions, *Pure appl. Geophys.,* **159**(10), 2429–2467.

Toda, S., Stein, R.S., Richards-Dinger, K. & Bozkurt, S., 2005. Forecasting the evolution of seismicity in southern California: animations built on earthquake stress transfer, *J. geophys. Res.,* **110,** B05S16.

Walsh, J.B. & Rice, J.R., 1979. Local gravity changes resulting from deformation, *J. geophys. Res.,* **84**(B1), 165–170.